Inorganic Chemistry

Article

pubs.acs.org/IC

New Type of Single Chain Magnet: Pseudo-One-Dimensional Chain of High-Spin Co(II) Exhibiting Ferromagnetic Intrachain Interactions

V. Tangoulis,*[†] M. Lalia-Kantouri,*[†] M. Gdaniec,[‡] Ch. Papadopoulos,[†] V. Miletic,[§] and A. Czapik[‡]

[†]Department of Chemistry, Laboratory of Inorganic Chemistry, Aristotle University, Thessaloniki 54 124, Greece

[‡]Faculty of Chemistry, Adam Mickiewicz University, 60780 Poznan, Poland

[§]Institute of Chemistry, Faculty of Sciences, University of Kragujevac, 34000 Kragujevac, Serbia

Supporting Information

ABSTRACT: Two new six-coordinated high-spin Co(II) complexes have been synthesized through the reactions of Co(II) salts with dipyridylamine (dpamH) and 5-nitro-salicylaldehyde (5-NO_2-saloH) or 3-methoxy-salicylaldehyde (3-OCH_3-saloH) under argon atmosphere: $[Co(dpamH)_2(5\text{-}NO_2\text{-}salo)]NO_3$ (**1**) and $[Co(dpamH)_2(3\text{-}OCH_3\text{-}salo)]NO_3 \cdot 1.3\ EtOH \cdot 0.4H_2O$ (**2**). According to the crystal packing of compound **1**, two coordination cations are linked with two nitrate anions into a cyclic dimeric arrangement via N−H···O and C−H···O hydrogen bonds. In turn, these dimers are assembled into (100) layers through $\pi-\pi$ stacking interactions between inversion-center related pyridine rings of the dpamH ligands. The crystal packing of compound **2** reveals a 1D assembly consisting solely from the coordination cations, which is formed by $\pi-\pi$ stacking interactions between pyridine rings of one of the dpamH along the [010] and another 1D assembly of the coordination cations and nitrate anions through the N−H···O hydrogen-bonding interactions along the [001] direction. All complexes were magnetically characterized, and a new approximation method was used to fit the magnetic susceptibility data in the whole temperature range 2−300 K on the basis of an empirical expression which allows the treatment of each cobalt(II) ion in axial symmetry as an effective spin $S_{eff} = {}^1/_2$. In zero-field, dynamic magnetic susceptibility measurements show slow magnetic relaxation below 5.5 K for compound **2**. The slow dynamics may originate from the motion of broad domain walls and is characterized by an Arrhenius law with a single energy barrier $\Delta_r/k_B = 55(1)$ K for the [10−1488 Hz] frequency range. In order to reveal the importance of the crystal packing in the SCM behavior, a gentle heating process to 180 °C was carried out to remove the solvent molecules. The system, after heating, undergoes a major but not complete collapse of the network retaining to a small percentage its SCM character.

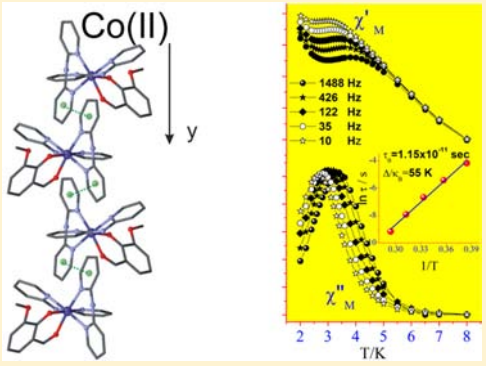

INTRODUCTION

Single-chain magnets (SCMs) are magnetically isolated chains possessing a finite magnetization that can be frozen in the absence of an applied magnetic field. At low temperatures, these systems can be considered as a magnet since the relaxation of the magnetization becomes significantly slow. A purely one-dimensional (1D) system does not exhibit any long-range ordering at a finite temperature,[1] but it is possible to obtain magnet behavior with a very slow relaxation. In 1963, R. J. Glauber predicted that slow magnetic dynamics can be obtained by considering chains combining a large magnetic anisotropy and ferromagnetic interactions.[2] The first experimental observation was only reported in 2001 in the $[Co^{II}(hfac)_2$. NITPhOMe] polymer where hfac = hexafluoroacetylacetonate and NITPhOMe = 4′-methoxy-phenyl-4,4,5,5,-tetramethylimidazoline-1-oxyl-3-oxide.[3] It has been shown that the measured slow relaxation of the magnetization and hysteresis effects are not associated with long-range order (LRO) in this compound. At the same time similar observations have been reported for chains of ferromagnetically coupled anisotropic $S = 3$ spin units.[4]

However, the observation of slow relaxation of the magnetization in ordered phases of ferrimagnetic chains was reported in 2002.[5] In these compounds, slow dynamics can either occur at the LRO transition temperature or at lower temperature, depending on the nature of both the 3D-metal spin and the organic spin. It was found that the LRO phenomena appear at a quite large temperature of 45 K while the SCM-like behavior appears around 10 K. In 2009 it was found[6,7] that SCM behavior can still occur in an antiferromagnetically ordered phase of spin chains where a Néel transition appears first and the SCM slow dynamics is observed at lower temperature. Finally, in 2011, it was shown that a 2D metamagnetic compound composed of ferromagnetic Co(II) chains can exhibit the slow relaxation of SCMs either in the antiferromagnetic ordered phase or in the field-induced ferromagnetic phase.[8]

In order to investigate new synthetic routes for the isolation of SCM systems, two new six-coordinated high-spin Co(II)

Received: March 5, 2013
Published: May 15, 2013

complexes were synthesized through the reactions of Co-$(NO_3)_2{\cdot}6H_2O$ with dipyridylamine (dpamH) and 5-nitro-salicylaldehyde (5-NO_2-saloH) or 3-methoxy-salicylaldehyde (3-OCH_3-saloH) under proper conditions in argon atmosphere, $[Co(dpamH)_2(5\text{-}NO_2\text{-}salo)]NO_3$ (**1**) and $[Co(dpamH)_2(3\text{-}OCH_3\text{-}salo)]NO_3{\cdot}1.3EtOH{\cdot}0.4H_2O$ (**2**). It must be pointed out that until now there are only two reports of Co(II) complexes with salicylaldehydes.[9,10] The complexes were characterized by physicochemical methods, and by IR spectroscopy and X-ray diffraction. The variable temperature magnetic measurements were undertaken for all the complexes, while the thermal stability and decomposition mode was studied in nitrogen atmosphere by using the simultaneous TG/DTG-DTA technique in nitrogen for compound **2**.

EXPERIMENTAL SECTION

All complexes were prepared under argon conditions, and well-degassed solutions have been used to avoid oxidation of the cobalt. The two cationic mixed-ligand complexes $Co(dpamH)_2(X\text{-}salo)]^+$ were prepared according to the following general procedure, under argon atmosphere, while well degassed solutions were used to avoid oxidation of the cobalt.[11] To an ethanolic solution (20 mL) of 291 mg of hexahydrate cobalt(II) nitrate was added 342 mg of dpamH under stirring and dropwise an ethanolic solution of 167 mg for 5-nitro-salicylaldehydeH and/or 152 mg for 3-methoxy-salicylaldehydeH substituted salicylaldehyde and 101 mg or 0.14 mL NEt_3. The solution was refluxed for 2 h until a clear transparent solution appeared. A dark orange solid was formed after several days. The solid was filtered; washed with water, cold ethanol, and diethylether; and dried under vacuum. The compounds prepared are soluble in hot EtOH, DMF, and DMSO and were found to have conductivity values in DMF solutions between 80.0 and 85.0 μS/cm, denoting their ionic character as 1:1 electrolytes.[12]

$[Co(dpamH)_2(5\text{-}NO_2\text{-}salo)]NO_3$ (1). Dark orange microcrystalline solid with stoichiometry calculated for $C_{27}H_{22}N_8O_7Co$: C, 51.51; H, 3.49; Co, 9.38; N, 17.80. Found: C, 51.25; H, 3.66; Co, 9.25; N, 17.61%. IR spectrum (KBr), selected peaks in cm^{-1}: 3295m, 3202m, and 3130m ν(N−H), 1618s ν(C═O), 1637s δ(N−H), 1580s ν(C═N), 1541 and 1325s of the NO_2, 1384s of the NO_3 ion, 853m and 725s (pyridyl C−H), 548m ν(Co−O), 424m ν(Co−N).

$[Co(dpamH)_2(3\text{-}OCH_3\text{-}salo)]NO_3{\cdot}1.3$ EtOH·0.4 H_2O (2). Orange-brown crystalline solid with stoichiometry calculated for $C_{28}H_{25}N_7O_6Co{\cdot}1.3C_2H_5OH{\cdot}0.4H_2O$: C, 53.87; H, 4.93; Co, 8.66; N, 14.38. Found: C, 53.55; H, 4.81; Co, 8.45; N, 14.22%. IR spectrum (KBr), selected peaks in cm^{-1}: 3295m, 3202m and 3130m ν(N−H), 2858m ν(C−H) of the OCH_3, 1618s ν(C═O), 1637s δ(N−H), 1580s ν(C═N), 1384s of the NO_3 ion, 853m and 725s (pyridyl C−H), 548m ν(Co−O), 424m ν(Co−N).

Physical Measurements. Microanalyses were carried out using a Perkin-Elmer 240 B CHN microanalyzer and Perkin-Elmer 5100 PC atomic absorption spectrophotometer for the metal content. Infrared spectra in the region of 4000−200 cm^{-1} were obtained in KBr discs with a Nicolet FT-IR 6700 spectrophotometer. Electronic absorption spectra (UV−vis) in Nujol were obtained on a Shimatzu 160A spectrometer. Molar conductivities were measured in DMF solutions, employing a WTW conductivity bridge and a calibrated dip type cell. Direct current and ac magnetic susceptibility measurements were carried out on polycrystalline samples with a DSM5 Quantum Design susceptometer working in the range 30−300 K under external magnetic field of 0.3 T and under a field of 0.03T in the 30−2 K range to avoid saturation effects. The simultaneous TG/DTG-DTA curves were obtained on a SETARAM thermal analyzer, model SETSYS-1200. The sample of approximately 10 mg was heated in platinum crucible, in an argon atmosphere at a flow rate of 80 mL min^{-1}, within the temperature range 30−1000 °C, at a heating rate of 10 °C min^{-1}.

Magnetic Models and Computational Details. For the sake of completeness a description will be given of the approximation method that has been used for the interpretation of the magnetic data developed by F. Lloret et al.[13,14] In general for a Co(II) ion in distorted octahedral symmetry there is a break of the degeneracy of the triplet orbital state $^4T_{1g}$ (case of axial distortion, D_{4h} point group). The Hamiltonian formalism is described in the following equation (eq 1)

$$\hat{H} = \alpha\lambda\hat{L}\hat{S} + \Delta\left[\hat{L}_Z^2 - \frac{1}{3}L(L+1)\right] + (-\alpha\hat{L} + g_e\hat{S})\beta H \quad (1)$$

where the first term is the spin−orbit coupling, the second term is related to the orbital distortion of the triplet ($L = 1$) in the case of an axial distortion, and the third term describes the Zeeman contribution. Moreover the α parameter is defined as the product of two other parameters κ and A ($\alpha = \kappa A$) which are responsible for the orbital reduction. The κ parameter, orbital reduction factor, is related to the covalency of the metal−ligand bonds and takes values in the range $0 \leq \kappa \leq 1$ while typical values for a six-coordinated high-spin Co(II) ion are in the range 0.70−0.95. The A parameter deals with the interaction of the $^4T_1$ levels from the ^4F and ^4P terms. This interaction causes admixtures between the $^4T_1(P)$ level and the ground $^4T_1(F)$ which are ligand-field dependent. The A values, for the weak and strong field conditions, are $A = {}^3/_2$ and $A = 1$, respectively, while in general its value is determined from optical spectra of the six-coordinated Co(II) complexes. F. Lloret et al.[13] developed an empirical expression dependent on λ, α, and Δ parameters since an exact analytical expression of the magnetic susceptibility of a Co(II) in a distorted octahedral geometry cannot be derived. According to this expression the ground doublet can be described through an effective spin, $S_{eff} = {}^1/_2$, using a temperature dependent function $G(T)$ instead of a constant g_0 Lande factor in order to apply the equation in the whole temperature range. This function takes into account the population of the excited states in an empirical way. The expression of $G(T)$ is given in eq 2

$$G(T) = \frac{\sum_{k=0}^{4}[\prod_{j=1}^{3}(\sum_{i=0}^{2}A_{i,j,k}x_j^i)T^k]}{\sum_{k=0}^{4}[\prod_{j=1}^{3}(\sum_{i=0}^{2}B_{i,j,k}x_j^i)T^k]} \quad (2)$$

where $x_1 = \alpha$, $x_2 = \Delta$ (cm^{-1}), $x_3 = \lambda$ (cm^{-1}), and T is temperature in Kelvin. A set of $\chi_M T$ versus T curves was simulated after numerical diagonalizations for several sets (α, Δ, λ) using the following modified susceptibility equation (eq 3)

$$\chi_M T = \frac{N\beta^2}{4k}|G(T)|^2 \quad (3)$$

The coefficients obtained from the expression of eq 2 are given elsewhere[13] for the cases of $\Delta > 0$ and $\Delta < 0$. This approximation is valid for α, Δ, λ parameters in the range 0−1000 ($|\Delta|$ in cm^{-1}), 0.75−1.5 (α), and 90−180 ($|\lambda|$ in cm^{-1}) and temperature range between 2 and 300 K.

For polynuclear complexes of Co(II) the Hamiltonian formalism is shown in eq 4

$$\hat{H} = -\sum_{i=1}^{n}J_i\hat{S}_i\hat{S}_{i+1} - \sum_{i=1}^{n}\alpha_i\lambda_i\hat{L}_i\hat{S}_i + \sum_{i=1}^{n}\Delta_i[\hat{L}_{zi}^2 - \frac{2}{3}] + \beta H\sum_{i=1}^{n}(-\alpha_i\hat{L}_i + g_e\hat{S}_i) \quad (4)$$

where the first term describes the isotropic exchange interaction between the Co(II) ions and all the others have the usual meaning described before. Although an "effective dimers" approach can be used to handle the above equation, the problem becomes intractable when the number of magnetic ions is increased. Instead, in order to derive an analytical expression for the magnetic susceptibility valid in the whole temperature range, Lines[15] used an approach for the case of ideal octahedral environment and F. Lloret et al.[13] used a perturbational approach for the low-symmetry environments which are the most common cases. This perturbational approach is valid when the magnetic coupling (J) is smaller than the spin−orbit coupling (λ) ($|J/\lambda| \ll 1$), which is also a common case among polynuclear compounds of Co(II). According to this approach, exchange coupling is between

dx.doi.org/10.1021/ic400557f | Inorg. Chem. 2013, 52, 6559−6569

ground Kramers doublet of each interacting ion and the Lande g_0 factor is replaced by the function $G(T)$ described earlier while contributions of excited levels on the magnetic properties are accounted using perturbation theory.

The $G(T)$ function has to be modified in order to take into consideration the influence of the exchange coupling of the excited states on the value of the Lande factor of the ground doublet of each Co(II) ion. Palii et al.[16] reported the variation Δg of the g_0 factor for the case of a Co(II) dimer (eq 5), and *a priori* this equation is still valid for each magnetic interaction within a polynuclear compound.

$$\tilde{g} = \frac{g_{\parallel} + 2g_{\perp}}{3} = g_0 + \Delta g$$
$$\Delta g = -\frac{100J}{81\alpha\lambda}(\alpha + 2) \quad (5)$$

A second modification of the $G(T)$ function is also applied where the temperature dependence of the Δg is included using a population actor P_0 (eq 6) from the low lying doublet under the assumption that excited states depending on Δ are averaged.

$$P_0 = \frac{\exp\left(-\frac{4\alpha\lambda}{kT}\right)}{3 + 2\exp\left(-\frac{5\alpha\lambda}{kT}\right) + \exp\left(-\frac{4\alpha\lambda}{kT}\right)} \quad (6)$$

According to the previous considerations, the $G(T)$ function is replaced by the $G(T, J)$ function (eq 7).

$$G(T, J) = G(T) + \frac{n}{2}\Delta g P_0 \quad (7)$$

Here, n is the average number of Co(II)−Co(II) interactions of each Co(II) ion in a polynuclear cluster (i.e., n takes values 1, 2, $^3/_2$ for a dimer, triangle, linear trinuclear).

The calculation of the magnetic susceptibility of a polynuclear compound requires every Co(II) to be treated as a spin doublet $S = {}^1/_2$ with the value of the $G(T, J)$ as the modified Lande factor while the analytical expression of the magnetic interaction can be calculated using well-known methods like for instance the Kambe's[17] method or numerical expressions.

For the case of an 1D ferromagnetic chain of Co(II) ions the analytical expression of the magnetic interaction can be taken from the well-known formula given by Baker et al.[18] for Heisenberg ferromagnetic $S = {}^1/_2$ chains (eq 8) where $A = 1 + 5.797\,9916x + 16.902\,653x^2 + 29.376\,885x^3 + 29.832\,959x^4 + 14.036\,918x^5$ and $B = 1 + 2.797\,9916x + 7.008\,678x^2 + 8.653\,8644x^3 + 4.574\,3114x^4$, $x = J/2kT$, and replacing the Lande factor with the new function $G(T, J)$.

$$\chi_M T = \frac{N\beta^2}{4k}|G(T, J)|^2\left(\frac{A}{B}\right)^{2/3} \quad (8)$$

The formula of eq 8 is going to be used for the magnetic interpretation of compound **1** while for compound **2** eq 3 is employed.

X-ray Crystallography. The diffraction data for single crystals were collected at 130 K with an Oxford Diffraction XcaliburE diffractometer using Mo Kα radiation for compound **1** and with an Oxford Diffraction SuperNova diffractometer using Cu Kα radiation for compound **2**. Single crystals of **1** and **2** with dimensions 0.41 × 0.22 × 0.09 mm^3, 0.10 × 0.02 × 0.02 mm^3, respectively, were taken directly from the mother liquid and immediately cooled to 130 K. The intensity data were collected and processed using CrysAlisPro software.[19] The structures were solved by direct methods with the program SHELXS-97[20] and refined by full-matrix least-squares method on F^2 with SHELXL-97.[20] The carbon-bound hydrogen atoms were refined as riding on their carriers, and their displacement parameters were set equal to 1.5U_{eq}(C) for the methyl groups and 1.2U_{eq}(C) for the remaining H atoms. The N−H group hydrogen atoms were located in electron difference maps and freely refined. In **3** one of the ethanol molecules has partial occupancy of 0.3, as was revealed by the refinement of its occupancy factors. Moreover, a peak located very close to the position of this ethanol oxygen atom indicated a possible presence of a water molecule. Occupancy factor of the water oxygen atom refined at 0.4. Disordered ethanol and water molecules shared in common one hydrogen atom for which 0.7 occupancy was assumed. Crystallographic data, data collection, and refinement details are given in Table 1. Molecular graphics were generated with ORTEP-3 for Windows[21] and Mercury 4.0 software.[22]

Table 1. Crystallographic Data, Data Collection, and Refinement Details for Compounds 1 and 2

	1	2
empirical formula	$[Co(dpamH)_2(5\text{-}NO_2\text{-}salo)]\,NO_3$	$[Co(dpamH)_2(3\text{-}OCH_3\text{-}salo)]\,NO_3{\cdot}1.3EtOH{\cdot}0.4H_2O$
CCDC no.	CCDC 919255	CCDC 919256
fw	629.46	681.57
cryst syst	triclinic	monoclinic
T	130 K	130 K
radiation	Mo Kα	Cu Kα
space group	$P\bar{1}$	$P2_1/c$
unit cell dimensions	a = 10.2990(6) Å	a = 9.6928(1) Å
	b = 11.3482(7)Å	b = 11.5880(2) Å
	c = 12.5241(7) Å	c = 27.7355(6) Å
	α = 106.519(5)°	α = 90°
	β = 107.472(5)	β = 91.893(2)
	γ = 91.459(5)°	γ = 90°
V	1328.73(14) Å^3	3113.56(9) Å^3
Z, Z'	2, 1	4, 1
abs coeff	0.710 mm^{-1}	4.847 mm^{-1}
indep reflns/R_{int}	4673/0.0320	5483/0.0285
params/restraints	396/0	446/0
GOF	1.031	1.049
final R indices R2/wR2 (all data)	0.0531/0.0943	0.0464/0.1196
largest diff peak/hole (e Å^{-3})	0.69/−0.32	0.42/−0.62

RESULTS AND DISCUSSION

Infrared Spectroscopy. In the spectra of the free salicylaldehyde ligands the intense bands stemming from the stretching and bending vibrational modes of the phenolic OH around 3200 cm^{-1} and 1410 cm^{-1}, respectively, disappear from the spectra of all complexes indicating the ligand deprotonation.[23] Also, the bands originating from the C−O stretching vibrations at 1245−1285 cm^{-1} in the complexes exhibit positive shifts at 1342−1385 cm^{-1} while their intensity is enhanced appreciably denoting coordination through the aldehydo oxygen of the ligand. The band at ∼1640 cm^{-1} attributable to the carbonyl bond ν(C═O) of the free ligand, upon coordination, in the complexes is shifted to lower frequencies at ∼1615 cm^{-1} thus denoting the bidentate monoanionic character of the studied salicylaldehydo ligands. The intense band of the free dipyridylamine at 1600 cm^{-1} (which is dimeric in the solid state, the N−H being hydrogen bonded to a ring nitrogen) is attributed to the bending mode of N−H. This band is present at ∼1638 cm^{-1} upon coordination, denoting the neutral character of the dpamH in the complexes. The intense bands at ∼1580 cm^{-1}, attributable to the stretching vibration of C═N (aromatic bond), are present in all complexes. The band at 720 ± 15 cm^{-1}, ascribed to the rocking vibrations of the pyridyl C−H bonds and the band at 830 ± 20 cm^{-1}, attributable to the deformation vibrations of the pyridyl C−H bonds, disclosed the occurrence of the nitrogenous base in the studied compounds. The medium to

dx.doi.org/10.1021/ic400557f | Inorg. Chem. 2013, 52, 6559−6569

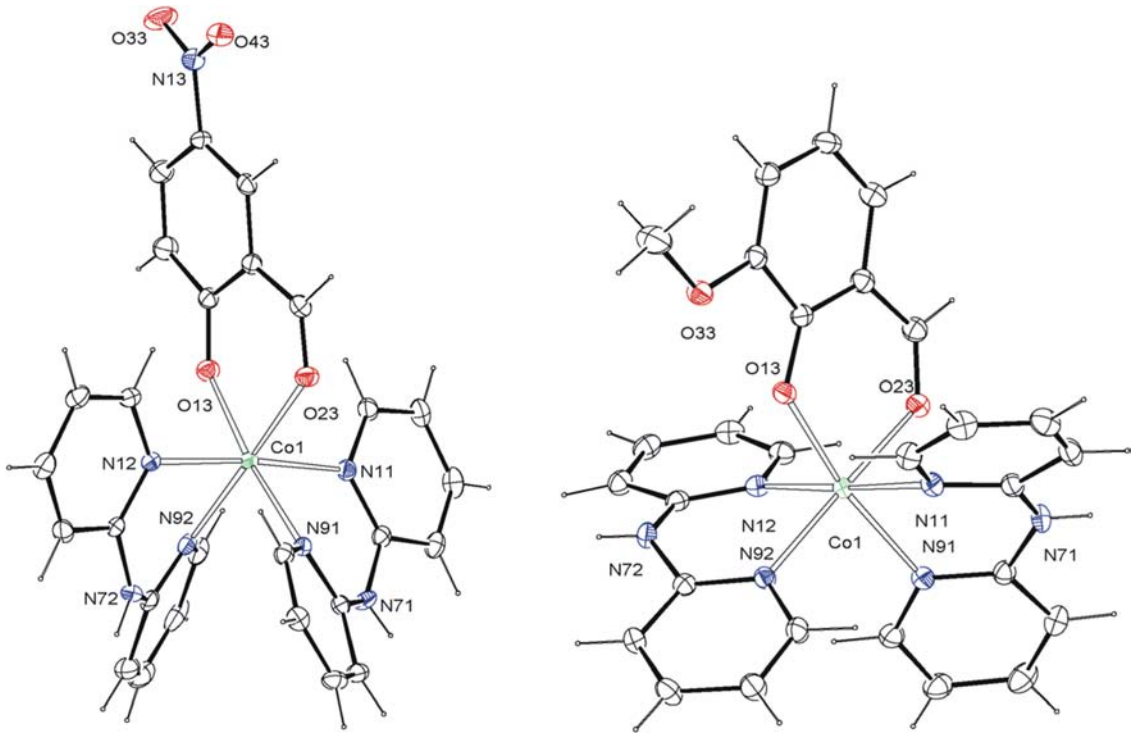

Figure 1. ORTEP plots at the 50% probability levels showing the coordination cations in compounds **1** (left) and **2** (right). The H atoms are drawn as small spheres of arbitrary size, and for clarity, only labels of Co, N, and O atoms are shown.

low intensity bands at 550 and 421 cm^{-1} are attributed to the coordination bonds (Co−O and Co−N, respectively) according to the literature.[24]

Electronic Spectroscopy. Cobalt(II) complexes have electronic spectra which are indicative of their stereochemistry. The ultraviolet−visible (UV−vis) spectra of the prepared complexes in the solid state as Nujol mulls, presented dominant bands in the region 50 000−9090 cm^{-1} (200−1100 nm). The bands in the UV region, present at wavelengths 38 000, 32 000 cm^{-1} (263, 312 nm) and 36 900, 27 700 cm^{-1} (271, 360 nm), are assigned to intraligand $\pi^* \leftarrow \pi$ or $\pi^* \leftarrow$n transitions, providing evidence arising from the position and intensity, as well as from the comparison with the spectra of the corresponding ligands, dpamH and salicylaldehydes. In the visible region, the three bands at 22 700−21 300, 18 500 (sh) cm^{-1} (440−468, 540 (sh)), and ∼10 000 cm^{-1} (∼1000 nm) are due to d−d transitions of the metal suggesting an octahedral arrangement of the ligands around Co(II).[25] The first band in the visible region steals intensity from the charge transfer band at ∼25 200 cm^{-1} (∼396 nm), which could be of MLCT character.

Description of the Structures. The molecular structures of the coordination cations in compounds $[Co(dpamH)_2(5\text{-}NO_2\text{-salo})]NO_3$ (**1**) and $[Co(dpamH)_2(3\text{-}OCH_3\text{-salo})]\text{-}NO_3\cdot 1.3\ EtOH\cdot 0.4H_2O$ (**2**) are shown in Figure 1, and their asymmetric units in Supporting Information (Figures S1 and S2). In both compounds, the cobalt(II) atom, chelated by one anionic salicylaldehyde-type ligand and two neutral dpamH molecules, is in a distorted octahedral coordination environment. The salicylaldehyde ligands coordinate in a typical mode, viz. through the phenolate and carbonyl oxygen atoms, forming six-membered chelate rings with the bite angles of 86.46(7)° and 89.28(7)° in **1** and **2**, respectively. The Co−N distances in the cations range from 2.107(2) to 2.162(2) Å (Table 2). In **2** the pair of *trans*-positioned Co−N bonds is somewhat longer [2.158(2), 2.162(2) Å] than the remaining two Co−N bonds [2.118(2), 2.131(2) Å]. In turn, the Co−O bond lengths formed by the phenolate groups [2.0290(19) and 2.0177(17) Å in **1** and **2**, respectively] are significantly shorter than those between Co^{II} and the carbonyl oxygens [2.1373(18) and 2.0888(17) Å in **1** and **2**, respectively]. The conformationally

Table 2. Relevant Bond Lengths and Angles for Compounds 1 and 2

	1	2
Bond Lengths (Å)		
Co1−N91	2.107(2)	2.131(2)
Co1−N92	2.119(2)	2.118(2)
Co1−N12	2.123(2)	2.158(2)
Co1−N11	2.134(2)	2.162(2)
Co1−O23	2.1373(18)	2.0888(17)
Co1−O13	2.0290(19)	2.0177(17)
Bond Angles (deg)		
O13−Co1−N91	173.73(8)	170.30(8)
O13−Co1−N92	94.66(8)	94.58(7)
N91−Co1−N92	90.60(8)	92.25(8)
O13−Co1−N12	92.27(8)	90.36(7)
N91−Co1−N12	91.71(8)	97.03(8)
N92−Co1−N12	83.65(8)	85.64(8)
O13−Co1−N11	91.60(8)	89.05(7)
N91−Co1−N11	84.73(8)	83.22(8)
N92−Co1−N11	92.68(8)	97.55(8)
N12−Co1−N11	174.87(8)	176.80(8)
O13−Co1−O23	86.46(7)	89.28(7)
N91−Co1−O23	88.47(8)	84.46(7)
N92−Co1−O23	176.72(8)	174.23(7)
N12−Co1−O23	93.23(8)	90.06(7)
N11−Co1−O23	90.37(8)	86.78(7)

dx.doi.org/10.1021/ic400557f | *Inorg. Chem.* 2013, 52, 6559−6569

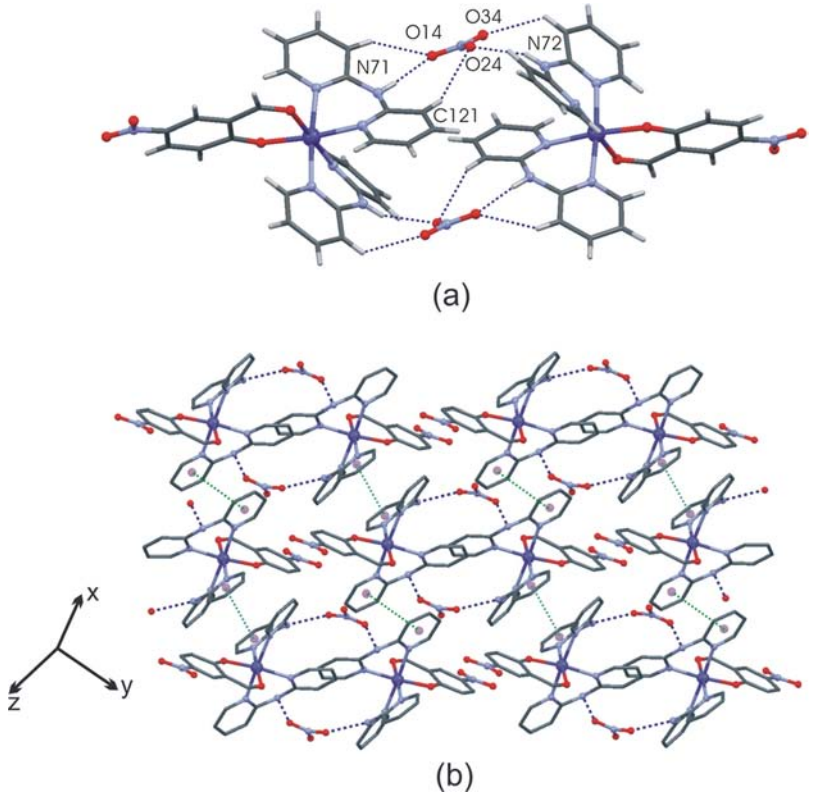

Figure 2. Intermolecular interactions in **1**: (a) N−H···O and C−H···O short contacts connecting two cations and two anions into centrosymmetric dimers; (b) the structure of the (100) layer formed through $\pi-\pi$ stacking interactions (green lines) between dpamH ligands from the hydrogen-bonded dimers. The two centroid−centroid distances are 3.800 and 3.858 Å.

flexible dpamH ligands adopt a butterfly shape with the dihedral angles between 2-pyridyl groups ranging from 23.04° to 31.55°. The boat shaped six-membered chelate rings formed by dpamH have the bite angles in the range 83.22(8)° to 85.64(8)°. Differences in the overall shapes of the coordination cations in **1** and **2** (Figure 1) result mainly from the inversion of the boat conformation of the six-membered chelate rings formed by *cis*-positioned dpamH ligands. These two structural forms with inverted boats are typical for bis-dpamH octahedral metal complexes and are nearly equally populated in the crystals.[11] The actual form adopted by the flexible dpamH ligands in the coordination entity is most probably affected by the crystal packing forces as in the two limiting forms the pair of N−H hydrogen-bond donor groups of dpamH ligands is oriented differently (Figure 1).

In crystals of **1**, two coordination cations are linked with two nitrate anions into a cyclic dimeric arrangement (Figure 2a) *via* N−H···O and C−H···O hydrogen bonds (Table 3). In turn, these dimers are assembled into (100) layers through $\pi-\pi$ stacking interactions between inversion-center related pyridine rings of the dpamH ligands. In one pair of stacked N11−C61 pyridine rings the interplanar distance is 3.477 Å and the centroid−centroid distance is 3.800 Å. In the other pair formed by the pyridine N92−C132 these parameters are 3.718 and 3.858 Å. The latter interaction brings two Co^{II} ions in this structure into the shortest distance of 7.751 Å. In turn, in **2**, where the two N−H groups on the cation are divergently directed, the N−H···O hydrogen-bonding interactions assemble the coordination cations and nitrate anions into chains extended along the [001] direction. Ethanol solvent molecules are attached to this chain *via* O−H···O interaction to the anion

Table 3. Geometrical Parameters (Å, deg) of Hydrogen Bonds of Compounds 1 and 2

D−H···A	*d*(D−H)	*d*(H···A)	*d*(D−A)	∠(D−H···A)
		1		
N71−H71···O14[a]	0.79(3)	2.09(3)	2.871(3)	173(3)
N72−H72···O24[b]	0.84(3)	2.15(3)	2.932(2)	156(3)
C31−H31···O14[a]	0.95	2.44	3.214(4)	139
C32−H32···O34[b]	0.95	2.52	3.164(4)	125
C131−H131···O24[a]	0.95	2.51	3.356(4)	148
C111−H111−O34[g]	0.95	2.47	3.133(4)	127
		2		
N71−H71···O24[c]	0.81(3)	2.07(3)	2.848(3)	161(3)
N72−H72···O14[d]	0.78(3)	2.11(3)	2.878(2)	167(3)
O15−H15···O24	0.84	2.13	2.826(5)	140
O16−H16···O15	0.83	1.96	2.794(11)	179
C42−H42···O33[e]	0.95	2.42	3.142(3)	133
C32−H32···O34[d]	0.95	2.48	3.431(4)	175
C26−H26···O34[f]	0.99	2.26	3.189(14)	156

[a]-Symmetry code: $-x+1, -y, -z+1$. [b]Symmetry code: $x, y+1, z$. [c]Symmetry code: $-x+1, -y+1, -z$. [d]Symmetry code: $-x+1, y-{}^1/_2, -z+{}^1/_2$. [e]Symmetry code: $-x+1, y+{}^1/_2, -z+{}^1/_2$. [f]Symmetry code: $-1+x, y, z$. [g]Symmetry code: $-x, -y, -z+1$.

(Figure 3a, Table 3). The distance of 13.891 Å between neighboring Co atoms along this chain is quite long. Another 1D assembly, consisting solely of the coordination cations, is formed by $\pi-\pi$ stacking interactions between pyridine rings of one of the dampH ligands (Figure 3b). This chain is extending along the [010] direction, and the distance between Co atoms is 8.784 Å. The geometric parameters, centroid−centroid

dx.doi.org/10.1021/ic400557f | *Inorg. Chem.* 2013, 52, 6559−6569

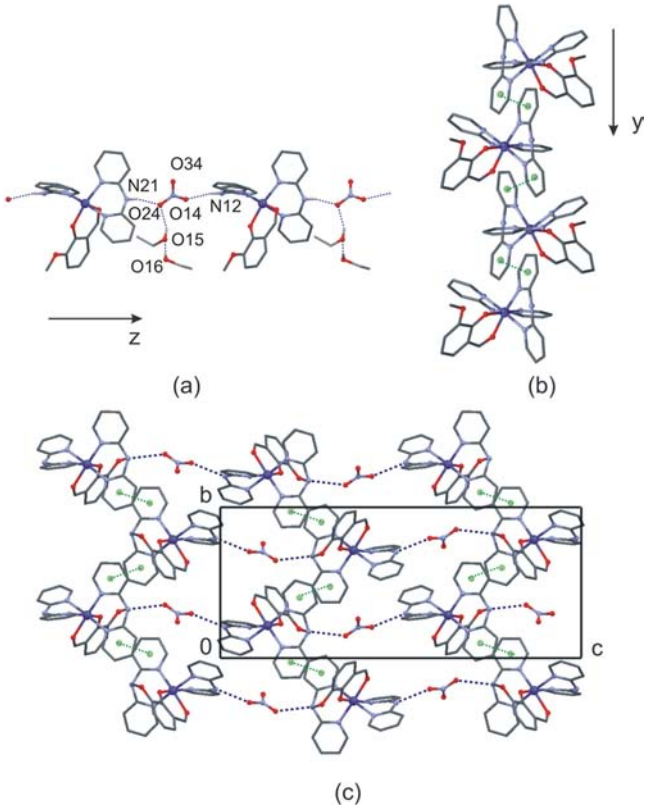

Figure 3. Intermolecular interactions in **2**: (a) the [001] chain formed *via* N−H···O interaction with the attached ethanol molecules (only H atoms involved in hydrogen bonding are shown); (b) the [010] chain of coordination cations formed through $\pi-\pi$ stacking interactions (green lines) between one of the dpamH ligands (H atoms omitted); (c) the (100) layer of cations and anions *via* hydrogen bonding and stacking interactions (solvent molecules are not shown).

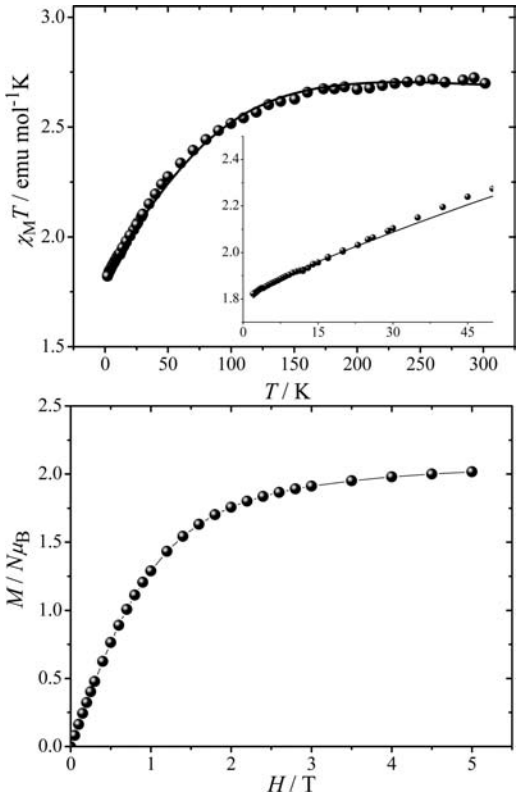

Figure 4. (Upper) Temperature dependence of the susceptibility data in the form of $\chi_M T$ for compound **1**. In the inset is shown the low temperature susceptibility data. Solid line represents the fitting results according to model discussed in the text. (Lower) Magnetization curve at 2 K of compound **1**. Solid line is guide for the eyes.

distance of 3.764 Å and interplanar distance of 3.31 Å, point to a relatively strong stacking interactions between the N11−C61 and N91−C131 pyridine rings along the chain. The two pyridine rings are arranged antiparallel which should additionally strengthen stacking interactions. The hydrogen-bonding interactions and $\pi-\pi$ stacking interactions organize the crystal components into (100) layers, and there are no specific interactions between molecules in adjacent layers.

Magnetic Properties of Compounds 1−2. The magnetic properties of compound **1** in the form of $\chi_M T$ versus T plot is shown in Figure 4. At room temperature, $\chi_M T$ is 2.75 emu mol^{-1} K, a value which is in agreement with a spin quadruplet with largely unquenched angular momentum.[26,27] Upon cooling, $\chi_M T$ slowly decreases until 100 K, and then, it decreases drastically reaching a value of 1.8 emu mol^{-1}K at 1.9 K. The decrease of $\chi_M T$ at high temperature is due to depopulation of the high energy Kramers doublets of the Co(II) ion. Using the theoretical model described earlier (eq 3), a least-squares fitting procedure was carried out, and the fitting result which is shown as solid line in the same figure is $\Delta = -947(10)$ cm^{-1}, $\lambda = -175(3)$ cm^{-1}, $\alpha = 1.11(1)$. The values of α, λ, Δ are within the range of those reported for high spin octahedral Co(II) complexes.[14]

The reduced magnetization $M/N\mu_B$ versus H at 2 K is also shown in the same figure. At 5 T the saturation value is 2.01 μ_B in agreement with the fact that only the ground Kramers doublet is populated at 2 K which can be associated with an effective spin $S_{eff} = {}^1/_2$ and $g = (10 + 2\alpha)/3$.[13]

Figure 5 shows the temperature dependence of the molar magnetic susceptibility for compound **2** in the form of $\chi_M T$ versus T using three different external magnetic field H = 30 to 300 to 5000 G. At room temperature, $\chi_M T$ is 3.68 emu mol^{-1} K, a value which is also in agreement with a spin quadruplet with largely unquenched angular momentum. Upon cooling, $\chi_M T$ slowly decreases until 25 K, and then it increases drastically reaching a value of 6.0 emu mol^{-1} K, respectively, at 5 K (at external field H = 30 G). The decrease of $\chi_M T$ at high temperature is due to depopulation of the high energy Kramers doublets of the Co(II) ion while the increase in the temperature range 5−25 K is due to ferromagnetic intrachain interaction between the Co(II) ions. Below 5 K there is a new decrease of the susceptibility data reaching the value of 4 emu mol^{-1}K at 1.9 K. In the same figure is shown the field dependence of the low temperature susceptibility data where it is clear that the maximum of the curve almost disappears at high magnetic fields while the zero-field-cooled (ZFC) and field-cooled (FC) measurements recorded under a field of 3 mT diverge below 5.0 K implying that long-range magnetic order appears at very low temperatures.

A recently developed "noncritical scaling" theory[28] was used to interpret the magnetic data which has shown that the minimum in the thermal variation of the χT product is well described by the sum of two exponential functions $\chi T = C_1 \exp(E_1/T) + C_2 \exp(E_2/T)$ where $C_1 + C_2$ is the high temperature extrapolated Curie constant. The fit of the magnetic susceptibility with this equation between 300 and 5

dx.doi.org/10.1021/ic400557f | Inorg. Chem. 2013, 52, 6559−6569

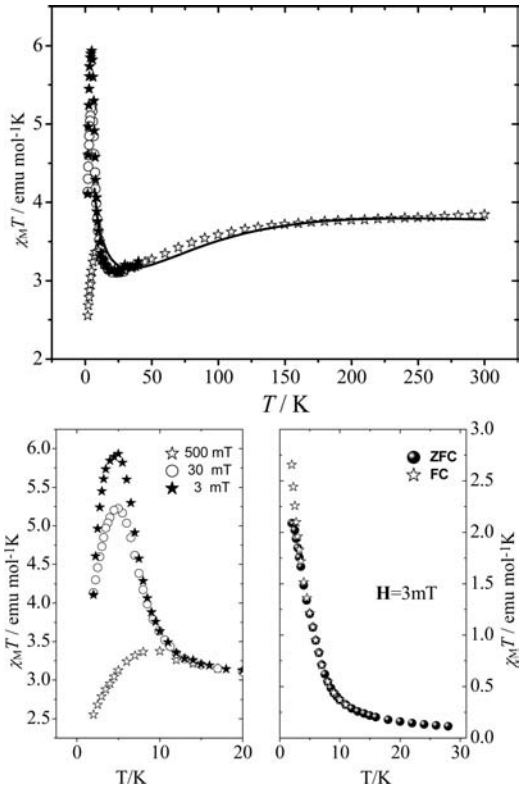

Figure 5. (Upper) Temperature dependence of the susceptibility data in the form of $\chi_M T$ for compound **2** at H = 3 (★), 30 (○), 500 (☆) mT. Solid line is the fitting result according to model described in eq 8. (Lower left) Low-temperature field dependent susceptibility data. (Lower right) ZFC-FC curves using an applied field H = 3mT.

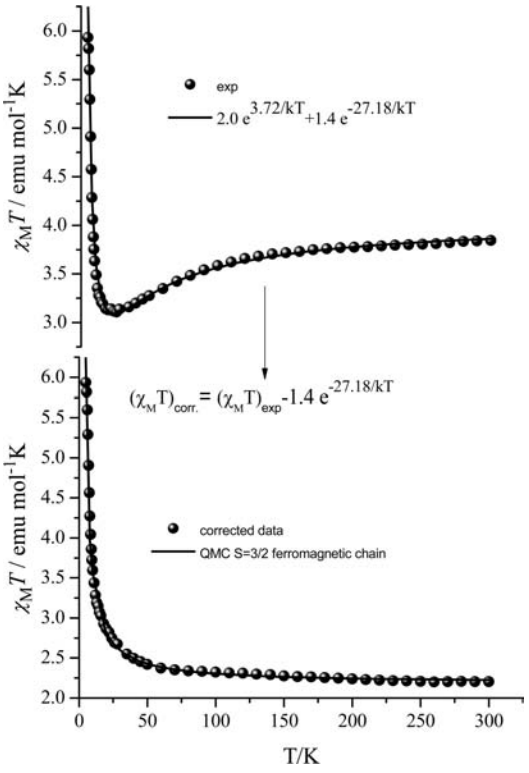

Figure 6. (Upper) Application of "noncritical scaling" theory for compound **2** in the susceptibility data and in temperature range 5−300 K (—). (Lower) QMC simulations of the corrected susceptibility data. See text for details.

K (Figure 6) yields C_1 = 2.00(7) emu K mol^{-1}, E_1 = −3.72(1) K, and C_2 = 1.40(4) emu K mol^{-1}, E_2 = 27.18(1) K. The extrapolated Curie constant $C_1 + C_2$ = 3.40 emu K mol^{-1} is in agreement with the expected values for octahedral Co(II) complexes. Here, the second term is a high-temperature antiferromagnetic contribution which represents the spin−orbit effects, whereas the first term is a low-temperature ferromagnetic contribution that corresponds to (a) the increase in the intrachain correlation length as described in the Ising model with, however, reduced effective spins because of partial compensation of the magnetic moments and (b) the ferromagnetic intrachain interactions.

To calculate the magnetic exchange interaction between Co(II) ions we subtracted the spin−orbit coupling effect from the experimental data.[29] A quantum Monte Carlo study[30] using the SSE algorithm[31] and based on the ALPS project[32] was carried out to simulate the resulting data. The obtained values are g = 2.16 and J = 1.8(1) cm^{-1}, indicating a moderate ferromagnetic interaction between the Co(II) ions through the $\pi-\pi$ stacking interactions between pyridine rings of one of the dampH ligands. Although this methodology of deriving the magnitude of exchange interaction in ferrimagnetic systems has been used earlier,[8,29] the results must be treated carefully and compared with other theoretical models in order to validate the physical meaning of the obtained parameters.

According to the theoretical model described earlier (eq 8), a second fit of the susceptibility data was employed, and the fitting results are Δ = −900(10) cm^{-1}, λ = −108(3) cm^{-1}, α = 1.4(1), J = 2.1(1) cm^{-1}. The values of α, λ, Δ are within the range of those reported for high spin octahedral Co(II) complexes, while the J value is close to the one obtained from the "noncritical scaling" theoretical approach. The results are shown as a solid line in Figure 4.

Alternating Current Magnetic Measurements. Dynamic ac magnetization measurements with frequencies ν in the 10−1500 Hz range have been performed in order to clarify the nature of the magnetic state of compound **2** and are shown in Figure 7. The thermal variation of the complex ac susceptibility shows rounded peaks for both the real and imaginary parts, while for the case of the real component a second peak maximum seems to emerge at temperatures lower than 2 K due to the onset of long-range ordering phenomena in agreement with the ZFC-FC measurements. Both in-phase and out-of-phase components show strong frequency-dependent behavior. χ' and χ'' shift to lower temperatures for lower frequencies which is expected for an SCM: as the temperature is lowered, correlations along the chain grow, and it becomes more difficult for the spins to follow the field. The shift of peak temperature (T_p) of χ'' is measured by a parameter $\varphi = (\Delta T_p/T_p)/\Delta(\log f)$ = 0.11, which is 2 orders larger than that for a canonical spin glass, closer to the value for a superparamagnet.[33] The temperature dependence of the relaxation time $\tau(t)$ follows the Arrhenius law: $\tau(t) = \tau_o \exp(\Delta_r/k_B T)$ and is shown in the same figure in the form of $\ln(\tau)$ versus $1/T$, where τ_o is a prefactor and Δ_r is the activation barrier. The fitted procedure gave the values Δ_r/k_B = 55 K and $\tau_o = 1.15 \times 10^{-11}$ s, in the range expected for SCM systems.[8,34]

The one-dimensional character of this compound can be verified further checking the correlation length, ξ, that is proportional to the (χT) product at zero dc field. In Figure 8 is shown the plot of $\ln(\chi T)$ versus $1/T$ in zero dc field from both

dx.doi.org/10.1021/ic400557f | Inorg. Chem. 2013, 52, 6559−6569

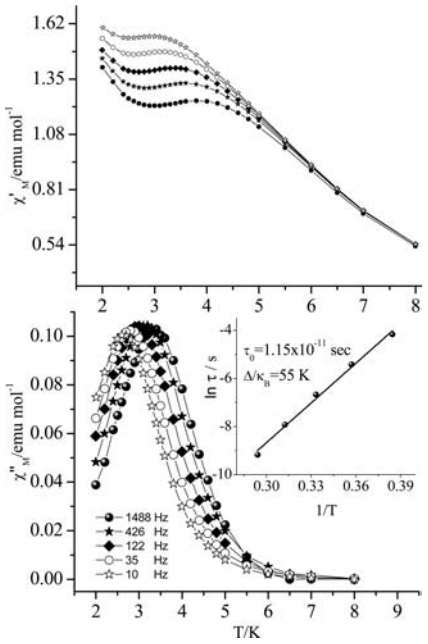

Figure 7. Temperature dependence ac magnetic susceptibility for compound **2** and for frequencies 10−1500 Hz. In the inset is shown the Arrhenius plot.

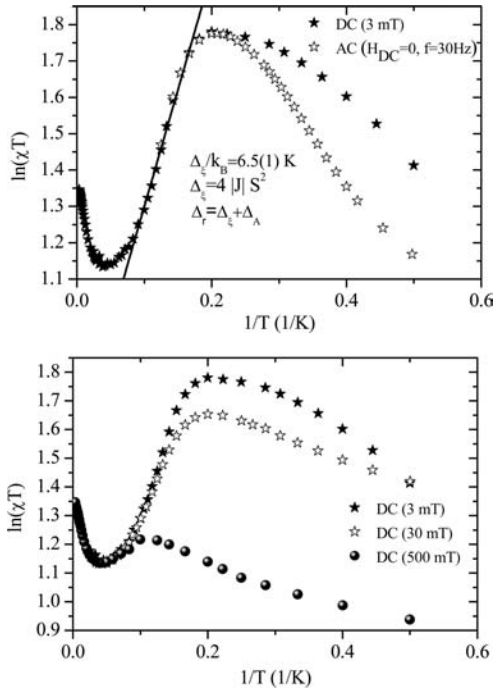

Figure 8. (Upper) Logarithmic representation of χT vs T^{-1} from ac 30 Hz (☆) and dc (★) data of compound **2**. The solid line represents the least-squares fit to the equation $\ln(\chi T) = \ln C_{eff} + \Delta_\xi/k_B\ (1/T)$. (Lower) Logarithmic representation of χT vs T^{-1} for different dc fields for compound **2**.

ac and dc measurements which has a linear part between 30 and 5 K, supporting an anisotropic Heisenberg or Ising-like 1D behavior. Deviations from this regime are observed at high and low temperatures possibly because of spin−orbit coupling effects and long-range phenomena, respectively. It has been shown that the χT product saturates in some 1D systems at low temperature due to finite size effects.[35] In our case there is an important decrease of the χT product at low temperatures (Figure 8, upper) while it strongly depends on the strength of the external field (Figure 8, lower). Neither the χT decrease in zero-field nor the strong field dependence of χT can be explained by a 1D model, in agreement with the proposed long-range phenomena possibly entered for temperatures lower than 2 K. This plot is used to extract the energy barrier Δ_ξ/k_B of creating domain walls. By linearly fitting the expression $\chi T = C_{eff} \exp(\Delta_\xi/k_B T)$, we extract the value $\Delta_\xi/k_B = 6.5(2)$ K. In the Ising limit this gap should be equal to $\Delta_\xi = 4|J|S^2$ giving an exchange constant $|J| = 4.5\ cm^{-1}$. Assuming $\xi > L$, L being the chain length, meaning the distance between two defects, the anisotropic barrier for the reversing of the magnetization of one spin can be calculated by the expression $\Delta_A/k_B = (\Delta_r - \Delta_\xi)/k_B$ (≈48 K). However, it is noticeable that this value of the exchange constant is of the order of magnitude of the exchange constants deduced by the noncritical scaling analysis and the approximation method.

Thermal Processing of Compound 2: TG-DTA and Magnetic Measurements. In order to investigate the role of the packing of the pseudo-1D chains, a sample of compound **2** was heated for two hours at 180 °C and the magnetic measurements have been recorded again. Moreover, the thermal behavior, by simultaneous thermogravimetric, derivative thermogravimetric and differential thermal analysis (TG/DTG-DTA) technique was undertaken for the same compound in nitrogen atmosphere at heating rate 10 °C min $^{-1}$, and the thermoanalytical curves are given in Figure 9. Using mass loss

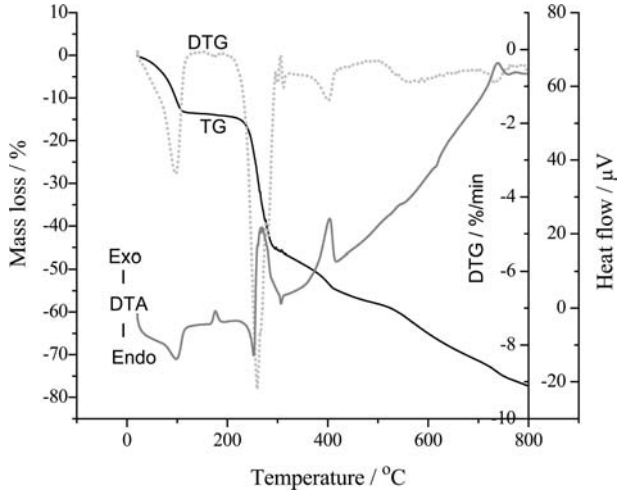

Figure 9. Thermoanalytical curves (TG/DTG-DTA) of compound **2** in nitrogen. Heating rate 10 °C min $^{-1}$.

and derivative mass loss plots (TG/DTG), we can conclude that, in the first stage (20−120 °C), compound **2** shows sudden mass loss (DTG peak at 97 °C and DTA endothermic peak at 98 °C) of 12.7%, which coincides with the release of the ethanol and water molecules, with a theoretical mass loss of 9.83%. The intermediate formed (desolvated compound) at 120 °C is stable until 230 °C, but it seems that a transformation without mass loss takes place at 176 °C, as the small exothermic peak on the DTA curve denotes. Upon increasing the temperature, the intermediate undergoes decomposition with subsequent sudden and gradual mass loses as follows: second stage [230−280 °C with DTG at 259 °C, DTA peaks at 252 °C (endothermic) and at 269 °C (exothermic)], and third stage

dx.doi.org/10.1021/ic400557f | Inorg. Chem. 2013, 52, 6559−6569

[280−500 °C, DTG peak at 401 °C, DTA at 407 °C (exothermic)]. Efforts to isolate the intermediates were not successful because of their continuous decomposition, as it was evidenced from the TG curves, while the mass losses (due to the elimination of the organic parts of the ligands and the nitrate ion) at these stages cannot be attributed to certain species. The amount of the solid material estimated from the TG curve was found to be 25.0% and denotes that the decomposition of this compound at 800 °C was not completed, since the calculated value for the expected metallic cobalt is 8.66% and for CoO 11.01%. These results are in accordance with those referred for other similar cobalt(II) complexes.[36,37]

Figure 10 shows the temperature dependence of the molar magnetic susceptibility for complex **2** after heat treatment in

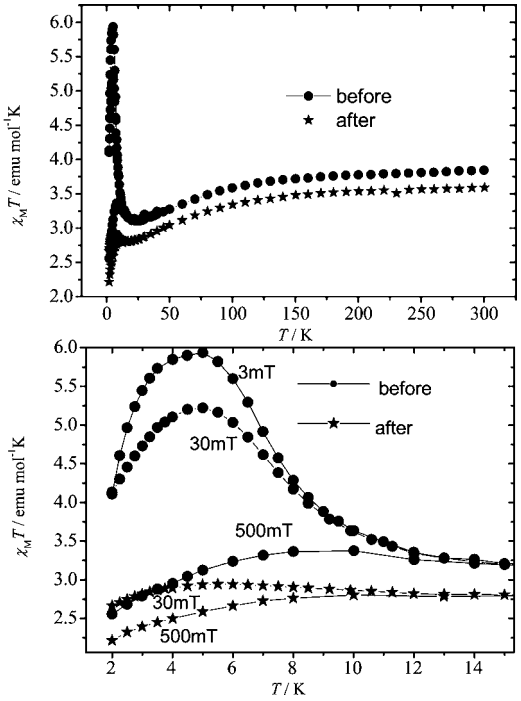

Figure 10. (Upper) Temperature dependence of the susceptibility data in the form of $\chi_M T$ for compound **2** after the heat treatment (★) at H = 30−5000 G along with the data (●) before the heat treatment. (Lower left) Low-temperature field dependent susceptibility data. (Lower right) Magnetization curves at 2 K.

the form of $\chi_M T$ versus T using two different external magnetic field H = 300−5000 G along with the data before the heat treatment for comparison reasons. The data suggest a structural transformation of the system with a completely different behavior which is in accordance to the TG-DTA measurements. At room temperature, $\chi_M T$ is 3.5 emu mol^{-1}K, and upon cooling, $\chi_M T$ slowly decreases until 25 K and then increases less drastically reaching a value of 3.0 emu mol^{-1} K, respectively, at 5 K. The decrease of $\chi_M T$ at high temperature is due to depopulation of the high energy Kramers doublets of the Co(II) ion while the increase in the temperature range 5−25 K is due to ferromagnetic interaction between the Co(II) ions. Below 5 K there is a new decrease of the susceptibility data reaching the value of 2 emu mol^{-1}K at 1.9 K. In the same figure is shown the field dependence of the low temperature susceptibility data where it is clear that the maximum of the curve disappears at high magnetic fields. The field dependence is still present but is less pronounced than before. According to the theoretical model described earlier (eq 8), a fit of the susceptibility data was employed, and the fitting results are Δ = −910(10) cm^{-1}, λ = −105(3) cm^{-1}, α = 1.5(1), J = 0.4(1) cm^{-1}. The values of α, λ, Δ are within the range of those reported for high spin octahedral Co(II) complexes and close to the values obtained for the compound **2** before the heat treatment. The major difference is the magnitude of the exchange interaction which is almost an order of magnitude smaller.

Dynamic ac magnetization measurements with frequencies ν in the 10−1500 Hz range have been performed in order to clarify the nature of the magnetic state of compound **2**. The thermal variation of the complex ac susceptibility shows rounded peaks for the case of the imaginary part, while for the case of the real component the peaks are almost unresolved. The actual magnitude of the imaginary part of susceptibility is almost 10 times smaller than before the heat treatment, and it is safe to assume that only a small percentage of the system (∼12%) retains its SCM character while most of it is paramagnetic.

Both in-phase and out-of-phase components show frequency-dependent behavior (Figure 11). The temperature dependence

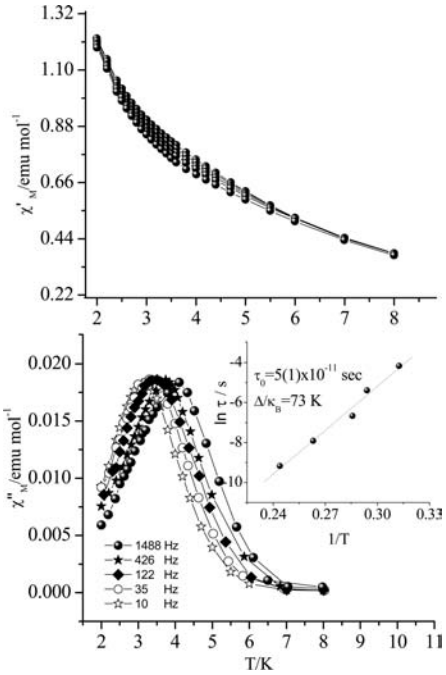

Figure 11. Temperature dependence ac magnetic susceptibility for compound **2** after the heat treatment for frequencies 10−1500 Hz. In the inset is shown the Arrhenius plot.

of the relaxation time $\tau(t)$ (Figure 11) follows the Arrhenius law, and the fitted procedure gave the values: Δ_r/k_B = 73(2) K and τ_o = 4.1(3) × 10^{-11} s. These calculations of the relaxation time and energy barrier of the percentage of the system behaving as an SCM may be erroneous since it is not certain if, after the heat treatment, this frequency dependence signal originates from real SCM systems or a mixture of them with SMM molecules of single Co(II) ions. Further investigation of the heat processing is needed in order to clarify this assumption.

The main difference between compounds **1** and **2** is the packing of the coordination cations. Compound **1** can be

dx.doi.org/10.1021/ic400557f | Inorg. Chem. 2013, 52, 6559−6569

described as pseudodimer (via N−H···O and C−H···O hydrogen bonds) assembled into chains through two different $\pi-\pi$ stacking interactions with interplanar distances 3.477 and 3.718 Å. Magnetic measurements showed that there is no interaction between the Co(II) ions which is in agreement with the crystallographic description of the system. For the case of compound **2** there is a pseudo-1D arrangement of the cations through $\pi-\pi$ stacking interactions between pyridine rings of one of the dampH ligands with interplanar distance of 3.31 Å while the distance between the Co(II) ions is 8.784 Å. To our knowledge it is the first time that this type of interaction yields a moderate strong ferromagnetic interaction according to the magnetic measurements. Also, this is the first time and remains an open question to be investigated further that the SCM character of a system is purely due to $\pi-\pi$ interactions. Hydrogen bonding interactions assemble the pseudo-1D chains and nitrate anions into a 2D layer where also ethanol solvent molecules are attached to this layer through hydrogen bonding. Nevertheless, the heat treatment of the system proves the importance of the packing conformation since after two hours of a thermal processing at 180 °C and the loss of the solvent molecules the magnetic behavior changed dramatically.

EPR Spectroscopy. X-band EPR measurements were carried out in powder samples of compounds **1** and **2** and are shown in Figure 12. As a consequence of the fast spin−

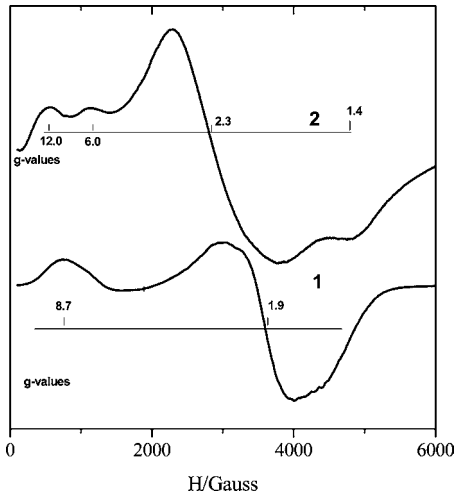

Figure 12. Powder X-band EPR spectra of compounds **1** and **2** at 4 K.

lattice relaxation time of high-spin Co(II), signals for compounds **1** and **2** were observed only below 100 K where for compound **1** a derivative centered at ca. g = 1.9 appears with a large peak centered at ca. g = 8.7 denoting no significant interactions between the Co(II) ions. The dominant broadening effect emerges when the g-strain is converted into B-strain through the equation $\Delta B = -((h\nu)/(\mu_B))((\Delta g)/(g^2))$, where the parameters have their usual meaning. Thus, the largest and smallest g-values of the powder spectra have field widths that differ by an order of magnitude, thereby rationalizing the broad high-field features of the spectrum. To explore the existence of a weak interaction between the Co(II) centers in compound **2**, X-band powder EPR experiments were carried out in the temperature range 4−100 K. The g values obtained from the powder EPR spectrum show large variations in the range 12.0−1.4 which is an indication of an exchange interaction between the Co(II) ions (Figure 12).

An important piece of information pertaining to the nature of the exchange interaction emerges from the g values of the single cobalt(II) ion. Therefore, if $g_z > g_x, g_y$, then the ion is closer to the Ising limit. Or, if $g_x, g_y > g_z$, then the system is closer to the XY limit. The conditions for observing $g_z > g_x, g_y$ were given earlier by Abragam and Bleaney, using a crystal field approach.[38] In that respect, it was found that in the Ising limit g_z= 8−9 and g_x= g_y= 0, while for the XY limit g_{xy}=4 and g_z= 2. The values observed here for compound **2** are beyond every limit, thus indicating that an interaction between the two Co(II) octahedral centers does arise in agreement with the above magnetic discussion.

CONCLUSIONS

Two new six-coordinated high-spin Co(II) complexes were synthesized through the reactions of Co(II) salts with dipyridylamine (dpamH) and 5-nitro-salicylaldehyde (5-NO_2-saloH) or 3-methoxy-salicylaldehyde (3-OCH_3-saloH): [Co(dpamH)$_2$(5-NO_2-salo)]NO_3 (**1**) and [Co(dpamH)$_2$(3-OCH_3-salo)]NO_3·1.3EtOH·0.4H_2O (**2**). The major difference between these compounds is the packing of the molecules, and while in the first case the magnetic studies showed that the Co(II) ions are magnetically isolated, in the second case a quite surprising SCM behavior is revealed due to pseudo-1D arrangement of the cations through $\pi-\pi$ stacking interactions between pyridine rings of one of the dampH ligands. Both in-phase and out-of-phase components show strong frequency-dependent behavior while the fitted procedure gave the values: Δ_r/k_B = 55 K and $\tau_o = 1.15 \times 10^{-11}$ s, concerning the activation barrier and the relaxation time, respectively. It was possible to calculate also the anisotropy barrier, Δ_A/k_B = 48 K, and the exchange constant between the magnetic ions $|J|$ = 4.5 cm^{-1}. The ferromagnetic interaction between the Co(II) ions has been further investigated using a new approximation method and a recently developed "noncritical scaling" theory while the obtained exchange constants are comparable to the one obtained from the ac measurements. Gentle heat treatment of compound **2** at 180 °C and the loss of solvent molecules yielded a major but not complete collapse of the network retaining to a small percentage its SCM behavior. In order to investigate further the salicylaldehydes ligands and the role of the packing of molecules, the synthesis of new compounds is underway where different transition metal ions (Ni(II), Mn(II), Fe(III)) will be used.

ASSOCIATED CONTENT

Supporting Information

Figures of the asymmetric units of compounds **1** and **2**. X-ray crystal structure refinement data for **1** and **2** in CIF format. This material is available free of charge via the Internet at http://pubs.acs.org.

AUTHOR INFORMATION

Corresponding Author

*E-mail: vtagkoul@chem.auth.gr (V.T.); lalia@chem.auth.gr (M.L.-K.). Phone: +30-2310-997-676 (V.T.); +30-2310-997-844 (M.L.-K.). Fax: +30-2310-996-196 (V.T.); +30-2310-997-844 (M.L.-K.)

Notes

The authors declare no competing financial interest.

REFERENCES

(1) (a) Coulon, C.; Miyasaka, H.; Clerac, R. *Struct. Bonding (Berlin)* **2006**, *122*, 163. (b) Miyasaka, H.; Julve, M.; Yamashita, M.; Clerac, R. *Inorg. Chem.* **2009**, *48*, 3420−3437.

(2) Glauber, R. J. *Math. Phys.* **1963**, *4*, 294.

(3) Caneschi, A.; Gatteschi, D.; Lalioti, N.; Sangregorio, C.; Sessoli, R.; Venturi, G.; Vindigni, A.; Rettori, A.; Pini, M. G.; Novak, M. A. *Angew. Chem., Int. Ed.* **2001**, *40*, 1760−1763.

(4) Clerac, R.; Miyasaka, H.; Yamashita, M.; Coulon, C. *J. Am. Chem. Soc.* **2002**, *124*, 12837.

(5) (a) Minguet, M.; Luneau, D.; Lhotel, E.; Villar, V.; Paulsen, C.; Amabilino, D. B.; Veciana, J. *Angew. Chem., Int. Ed.* **2002**, *41*, 586−589. (b) Lhotel, E.; Simonet, V.; Ressouche, E.; Canals, B.; Amabilino, D. B.; Sporer, C.; Luneau, D.; Veciana, J.; Paulsen, C. *Phys. Rev. B* **2007**, *75*, 104429.

(6) Coulon, C.; Clerac, R.; Wernsdorfer, W.; Colin, T.; Miyasaka, H. *Phys. Rev. Lett.* **2009**, *102*, 167204.

(7) Miyasaka, H.; Takayama, K.; Saitoh, A.; Furukawa, S.; Yamashita, M.; Clerac, R. *Chem.—Eur. J.* **2010**, *16*, 3656−3662.

(8) Zhang, X. M.; Wang, Y. Q.; Wang, K.; Gao, E. Q.; Liu, C. M. *Chem. Commun.* **2011**, *47*, 1815−1817.

(9) Pflunger, C. E.; Hon, P. K.; Harlow, R. L. *J. Cryst. Mol. Struct.* **1974**, *4*, 55−61.

(10) Xiao, Y.; Zhang, M. *Acta Crystallogr.* **2008**, *E64*, m1231.

(11) Lalia-Kantouri, M.; Gdaniec, M.; Choli-Papadopoulou, T.; Badounas, A.; Papadopoulos, C. D.; Czapik, A.; Geromichalos, G. D.; Sahpazidou, D.; Tsitouroudi, F. *J. Inorg. Biochem.* **2012**, *117*, 25−34.

(12) Geary, W. J. *Coord. Chem. Rev.* **1971**, *7*, 81−122.

(13) Lloret, F.; Julve, M.; Cano, J.; Ruiz-Garcia, R.; Pardo, E. *Inorg. Chim. Acta* **2008**, *361*, 3432−3445.

(14) Tudor, V.; Geanina, M.; Lloret, F.; Kravtsov, Ch. V.; Simonov, Y. A.; Julve, M.; Andruh, M. *Inorg. Chim. Acta* **2008**, *361*, 3446−3452.

(15) Lines, M. E. *J. Chem. Phys.* **1971**, *55*, 2977.

(16) (a) Palii, A. V.; Tsukerblat, B. S.; Coronado, E.; Clemente-Juan, J. M.; Borrass-Almenar, J. J. *Inorg. Chem.* **2003**, *42*, 2455. (b) Palii, A. V.; Tsukerblat, B. S.; Coronado, E.; Clemente-Juan, J. M.; Borrass-Almenar, J. J. *J. Chem. Phys.* **2003**, *118*, 5566.

(17) Kambe, K. *J. Phys. Soc. Jpn.* **1950**, *5*, 48.

(18) Baker, G. A., Jr.; Rushbrooke, G. S.; Gilbert, H. F. *Phys. Rev.* **1964**, *135* (5A), 1272.

(19) *CrysAlis PRO Software*; Agilent Technologies: Yarnton, Oxfordshire, U.K., 2011.

(20) Sheldrick, G. M. *Acta Crysallogr.* **2008**, *A64*, 112−122.

(21) Farrugia, L. J. *J. Appl. Crystallogr.* **1997**, *30*, 565.

(22) Macrae, C. F.; Edgington, P. R.; McCabe, P.; Pidcock, E.; Shields, G. P.; Taylor, R.; Towler, M.; van de Streek, J. *J. Appl. Crystallogr.* **2006**, *39*, 453−457.

(23) Silverstein, R. M.; Bassler, G. C.; Morvill, G. *Spectrometric Identification of Organic Compounds*, 6th ed.; Wiley: New York, 1998; p 87.

(24) Nakamoto, K. *Infrared and Raman Spectra of Inorganic and Coordination Compounds*, 5th ed.; Wiley-Interscience: New York, 1997.

(25) Lever, A. B. *Inorganic Electronic Spectroscopy*, 2nd ed.; Elsevier: New York, 1984; pp 480−490.

(26) (a) Mateescu, A.; Raptopoulou, C. P.; Terzis, A.; Tangoulis, V.; Salifoglou, A. *Eur. J. Inorg. Chem.* **2006**, 1945−1956. (b) Jankovics, H.; Daskalakis, M.; Raptopoulou, C. P.; Terzis, A.; Tangoulis, V.; Giapintzakis, J.; Kiss, T.; Salifoglou, A. *Inorg. Chem.* **2002**, *41*, 3366−3374. (c) Matzapetakis, M.; Dakanali, M.; Raptopoulou, C. P.; Tangoulis, V.; Terzis, A.; Moon, N.; Giapintzakis, J.; Salifoglou, A. *JBIC, J. Biol. Inorg. Chem.* **2000**, *5*, 469−474.

(27) (a) Rizzi, A. C.; Brondino, C. D.; Calvo, R.; Baggio, R.; Garland, M. T.; Rapp, R. E. *Inorg. Chem.* **2003**, *42*, 4409−4416. (b) Rodriguez, A.; Sakiyama, H.; Masciocchi, N.; Galli, S.; Galvez, N.; Lloret, F.; Colacio, E. *Inorg. Chem.* **2005**, *44*, 8399.

(28) (a) Drillon, M.; Panissod, P.; Rabu, P.; Souletie, J.; Ksenofontov, V.; Gutlich, P. *Phys. Rev. B* **2002**, *65*, 104404. (b) Souletie, J.; Rabu, P.; Drillon, M. *Phys. Rev. B* **2005**, *72*, 214427.

(29) Yoo, H. S.; Kim, J. I.; Yang, N.; Koh, E. K.; Park, E. K.; Hong, C. S. *Inorg. Chem.* **2007**, *46*, 9054−9056.

(30) An $S = {}^3/_2$ infinite chain model was used based on the spin Hamiltonian $H = -2JS_iS_{i+1}$ where for each site 5×10^6 Monte Carlo steps were performed and 10% of them were discarded as the initial transient stage while the sample was 300 spins. This sample is large enough to prevent any finite size effects. To avoid perturbation from the edge of the sample and to speed up convergence toward the infinite lattice limit, periodic boundary conditions (PBC) were used.

(31) (a) Sandvik, A. W.; Kurkijarvi, J. *Phys. Rev. B* **1991**, *43*, 5950. (b) Sandvik, A. W. *J. Phys. A* **1992**, *25*, 3667.

(32) ALPS Collaboration: Alet, F.; et al. *J. Phys. Soc. Jpn. Suppl.* **2005**, *74*, 30.

(33) Mydosh, J. A. *Spin Glasses: An Experimental Introduction*; Taylor & Francis: London, 1993.

(34) Sibille, R.; Mazet, T.; Malaman, B.; Gaudisson, T.; Francois, M. *Inorg. Chem.* **2012**, *51*, 2885−2892.

(35) Coulon, C.; Clerac, R.; Lecren, L.; Wernsdorfer, W.; Miyasaka, H. *Phys. Rev. B* **2004**, *69*, 132408.

(36) Ferenc, W.; Cristvao, B.; Sarzynski, J. *J. Therm. Anal.* **2010**, *101* (2), 761−767.

(37) Dziewulska-Kulaczkowska, A. *J. Therm. Anal.* **2010**, *101* (3), 1019−1026.

(38) Abragam, A.; Bleaney, B. In *Electron Paramagnetic Resonance of Transition Ions*; Clarendon Press: Oxford, U.K., 1970.